

Range-extended confocal chromatic sensor system for double-sided measurement of optical components with high lateral resolution

Christian Haider, Martin E. Fuerst, Matthias Laimer, Ernst Csencsics and Georg Schitter, *Senior Member, IEEE*

Abstract—This paper presents a strategy to break the tradeoff between the thickness measuring range of a confocal chromatic sensor (CCS) and its lateral imaging resolution. By combining the sensor with a linear stage, the thickness measuring range is no longer limited by chromatic dispersion, but by the focusing power of the sensor optics. The principle is demonstrated with a prototype setup that utilizes a CCS with a spot size of $6\ \mu\text{m}$ and a spec-sheet thickness measuring range of $300\ \mu\text{m}$. By implementing the proposed mechatronic approach, a successful extension of the measuring range by a factor of 17 is achieved while preserving the lateral resolution of $2.46\ \mu\text{m}$ for thickness measurements. The proposed measurement scheme is validated by measuring lateral surface features on a $1.2\ \text{mm}$ thick lenslet array from the backside.

Index Terms—opto-mechatronic system, range-extension, confocal chromatic sensor, surface metrology

I. INTRODUCTION

In many fields of modern industry, high-precision manufacturing of optical elements is of key importance [1]. The trend for downscaling optoelectronic devices calls for more efficient optical element designs, encouraging complex geometries [2]. Recent developments include displays for augmented reality [3], microlenses [4] and contact lenses with possible incorporation of wireless devices and sensors [5]. In order to validate the optical performance and ensure reliable manufacturing processes of these components, precise measurement systems are required [6].

The main methods that are used for surface metrology of optical parts are coordinate measuring machines (CMMs) [7, 8] and interferometric techniques [9, 10]. Both methods share a major drawback: They measure the shape of a single surface. This means that for a full characterization of an optical component, two subsequent one-sided measurements of both sides of the sample need to be conducted. Thus, information about the orientation of both surfaces relative to each other gets lost and potential angles between top and bottom surface profiles (wedge) cannot easily be determined. Additionally, it is difficult to preserve consistency between the measurement coordinates (e.g. rotational orientation) for subsequent measurements of top and bottom surface

The authors are with the Christian Doppler Laboratory for Precision Engineering for Automated In-Line Metrology at the Automation and Control Institute (ACIN), Vienna University of Technology, 1040 Vienna, Austria. Corresponding author: haider@acin.tuwien.ac.at

without adding mechanical reference artifacts (fiducials) to the sample [11].

A possible way to overcome these limitations is offered by the thickness measurement capability of the confocal chromatic sensor (CCS). A CCS uses chromatic aberration along the sensor's optical axis in combination with a detecting spectrometer to determine distance and thickness values [12]. In principle, the CCS thus enables a shape measurement of a transparent part from one side, which is also beneficial for samples, where only one-sided optical access is possible due to assembly constraints [13]. The CCS is commonly used for measuring the thickness of tissue samples [14] and films directly in the production line [15] or for refractive index measurements in harsh environments [16], as it is a fast and reliable sensor. In recent years, its applications have also been extended to optical surface metrology [17], motivating the development of precise profilometers [18, 8], and non-contact quality control [19]. In a novel application, a CCS is combined with a nano-positioning stage, enabling sub-aperture scanning and stitching of microstructures [20]. Another method combines a camera with a confocal chromatic sensor in order to monitor the measuring point [21]. The measuring range of a CCS is determined by its numerical aperture (NA), which is essentially the focusing angle of the emitted light, and the measuring range increases for sensors with lower NA. However, in order to achieve a high lateral imaging resolution, a small CCS spot size is needed, which can only be achieved with a higher NA [22]. This makes it difficult to measure small lateral surface features on the backside of a thick object, if optical access is restricted to one side or flipping of the sample is infeasible.

The contribution of this paper is the implementation of a mechatronic measurement range extension for a high-NA confocal chromatic sensor by combining it with a linear stage to axially reposition the sensor, allowing the measurement of thick samples exceeding the nominal measuring range of the CCS while maintaining a high lateral resolution. The combination of the CCS system with an XY-positioning system further enables point-by-point 3D surface measurements. The top and bottom surface can effectively be moved into measuring range subsequently, allowing the backside measurement of thicker samples with maintained CCS spot size and thus achieving the same lateral resolution as on the top surface.

II. MEASUREMENT CONCEPT

A. Confocal chromatic sensor working principle

A confocal chromatic sensor (CCS) uses longitudinal chromatic aberration for distance and thickness measurements with an axial resolution in the nanometer range [23]. The working principle is illustrated in Figure 1.

White light is emitted from a point source and dispersed through a lens stack, so that the spectral components are focused at different distances along the optical axis. The

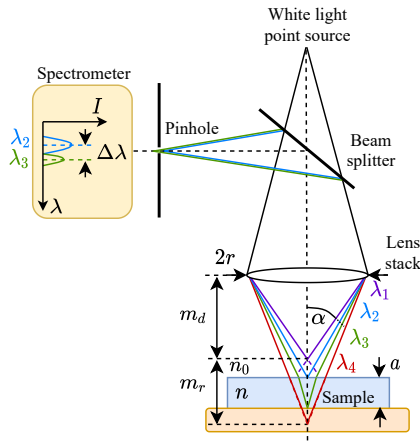


Fig. 1. Working principle of optical confocal chromatic sensor for thickness measurement. Reflected light from the top and bottom surface is diverted onto the pinhole, where only light in focus (λ_2 and λ_3) is able to enter, while the non-focused light (λ_1 , λ_4) is blocked. The corresponding intensity peaks in the spectrometer allow the calculation of the sample thickness a , provided that the refractive index n is known.

distance between the focus points of the shortest (λ_1) and the longest (λ_4) wavelength determines the measuring range m_r of the sensor. No measurement is possible within the offset distance from the lens aperture to the first focus point of λ_1 , in the following referred to as measuring distance m_d .

The light is reflected from the sample surface and redirected via a beam splitter towards a pinhole. If the sample is thinner than m_r , the bottom surface of the sample also lies within the focus region, resulting in two detectable peaks in the spectrometer. If the refractive index n of the sample is known, its thickness a can be calculated from the wavelength difference $\Delta\lambda$.

Furthermore, Snell's law of refraction effectively leads to a sample-related extension of the nominal measuring range m_r , scaled by the sample refractive index n to

$$m_{r,real} = n \cdot m_r, \quad (1)$$

determining the real thickness measurement limit for a given sensor and sample material [22].

B. The tradeoff between measuring range and lateral resolution

The lateral resolution and measuring range of confocal chromatic sensors are limited by diffraction and chromatic aberration, respectively. The lateral resolution R_{lat} can be defined as the inverse of the CCS measurement spot size d_{spot} , which in turn depends on the diffraction limit [22] and can thus be written as

$$R_{lat} = \frac{1}{d_{spot}} = \frac{2 \cdot NA}{\lambda}, \quad (2)$$

with $NA = n_0 \cdot \sin(\alpha)$. It can be clearly seen, that the lateral resolution increases with a higher NA. Assuming that the light source is located far from the lens stack compared to its focal length, the measuring range m_r can be characterized by the (wavelength-dependent) focal lengths f_S , f_L and f_C (focal length of shortest, longest and central wavelength). With the Lensmaker's equation [22] the amount of chromatic aberration produced by a lens can be quantified as

$$\frac{1}{f_S} - \frac{1}{f_L} = \frac{1}{f_C} \cdot \frac{1}{\nu}, \quad (3)$$

with the Abbe number ν as a material parameter. With this relation the measuring range m_r can be approximated as

$$m_r = f_L - f_S = \frac{f_S \cdot f_L}{f_C \cdot \nu} \approx \frac{f_C}{\nu} \approx \frac{m_d}{\nu}, \quad (4)$$

where the measuring distance $m_d \approx f_C$. The measuring distance m_d can be related to the sensor geometry (given by the lens diameter $2r$ and opening angle α) via

$$m_d = \frac{r \cdot n_0 \cdot \cos(\alpha)}{NA}. \quad (5)$$

This allows expressing m_r as

$$m_r \approx \frac{m_d}{\nu} = \frac{r \cdot n_0 \cdot \cos(\alpha)}{NA \cdot \nu}, \quad (6)$$

depending on sensor parameters. It can be seen that m_r decreases for a higher NA, making the product $R_{lat} \cdot m_r$ independent of NA

$$R_{lat} \cdot m_r = \frac{2r \cdot n_0 \cdot \cos(\alpha)}{\lambda \cdot \nu} \leq \frac{2r}{\lambda \nu}. \quad (7)$$

As long as the sensor is operated in air or vacuum, $n_0 = 1$. Further, since $\cos(\alpha) < 1$, an upper limit for the resolution-range product is given by

$$R_{lat} \cdot m_r \leq \frac{2r}{\lambda \nu} \quad (8)$$

and can only be maximized by increasing the lens diameter $2r$, since ν and λ are fixed. Increasing the size of optical elements, however, becomes immensely challenging and prohibitively expensive.

In Figure 2 a number of commercially available confocal chromatic sensors are compared, relating their lateral resolution to their measuring range [24]. The tradeoff $R_{lat} \cdot m_r$ is indicated by the dashed line, with parameters chosen to match the best-performing sensor (IFS2406-10, with $R_{lat} \cdot m_r = 666.66$,

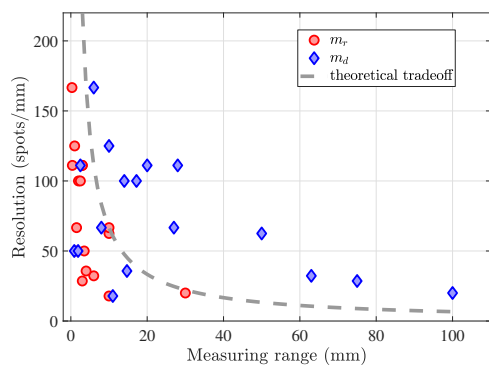


Fig. 2. The measuring range m_r and the measuring distance m_d versus the lateral resolution for various confocal chromatic sensor types [24]. The dashed line indicates the limiting tradeoff as described by Equation 8.

corresponding to $r = 6.97$ mm, $\alpha = 14.48^\circ$, $\lambda = 550$ nm and $\nu = 36.81$. The nominal measuring range (pictured in red) lies below this line for all other sensor models. However, it can be seen that the the measuring distance (in blue) lies above the dashed line for the majority of the sensors. A strategy to turn the measuring distance into the usable measuring range, thereby breaking the conventional tradeoff, is presented in the next section.

C. Range extension concept

In Figure 3 the tradeoff is illustrated for two exemplary sensors. In the first case, a low-NA sensor with a high measuring range m_r is capable of measuring the thickness of the sample, but the inevitably larger spot size limits the lateral resolution for detecting small structural features on the sample surfaces. In contrast, a high-NA sensor with a small spot size is able to measure surface features with high resolution, but the measuring range m_r is prohibiting a thickness measurement, as indicated in Figure 3b. The proposed solution, depicted in Figure 3c, is to extend the measuring range of such a system by repositioning the CCS along the optical axis. Thus, the top and bottom surface measurement data is acquired consecutively, effectively extending the CCS measuring range from m_r up to $m_r + m_d$. This enables the measurement of thick samples, while a small CCS spot size is maintained to achieve a high lateral imaging resolution for small features on both sample surfaces. By combining this measurement principle with an XY-positioning system to move the sensor or the sample in two dimensions while conducting a point by point scan, the true 3D shape of optical elements can be measured without flipping the sample.

The optical implications of this sensor concept are analysed in Figure 4. The sample thickness a is exceeding the measuring range m_r and a straightforward thickness measurement (and thereby shape measurement) is not possible.

However, by moving the CCS closer to the sample and recording the required shift Δz with an additional high-resolution

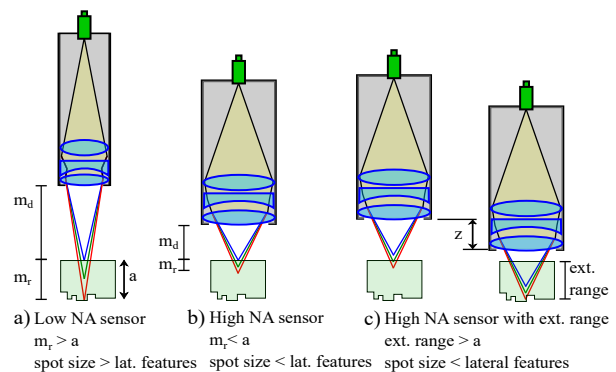


Fig. 3. CCS range extension principle. (a) A low-NA sensor is capable of measuring the thickness but is sacrificing lateral resolution due to the larger spot size. (b) A high-NA sensor measures with high lateral resolution, but entails a smaller m_r . (c) Proposed solution to overcome this tradeoff by axial repositioning of the sensor, enabling a subsequent measurement of both surfaces with preserved lateral resolution.

displacement sensor, the bottom surface is effectively moved back into measuring range. Thus, top and bottom surface can be measured by varying the sensor distance without moving or flipping the sample, while the lateral resolution is unaffected.

A geometric relation between the two focus points can be

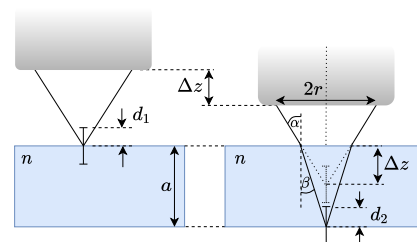


Fig. 4. Simplified case of extended thickness measurement illustrating the measurement of the bottom surface.

derived as [25]

$$\frac{\tan(\alpha)}{\tan(\beta)} = \frac{a}{\Delta z}. \quad (9)$$

By considering the distances d_1 and d_2 , measured by the CCS, the relation can be written as

$$\frac{\tan(\alpha)}{\tan(\beta)} = \frac{a}{\Delta z - d_1 + d_2}, \quad (10)$$

which results to

$$a = n(\Delta z - d_1 + d_2) \frac{\cos(\beta)}{\cos(\alpha)} \quad (11)$$

by applying Snell's law of refraction and assuming the refractive index of air being equal to one. The first term essentially corresponds to a scaling of the absolute measured distance by the sample's refractive index n , which is an adaption of the equation presented in [22, 26].

However, this approximation does not consider that the rays forming the convergent light beam exiting the aperture of the sensor are hitting the plane sample surface under different angles of incidence. The angle decreases from the outermost beam, which hits the surface under the aperture angle $\alpha_{\text{apt}} = \arcsin(\text{NA})$, to $\alpha = 0^\circ$ in the center [27]. This results in a spatial distribution of the focus along the optical axis depending on α , adding to the scaling of the focus due to the refraction. The term $\frac{\cos(\beta)}{\cos(\alpha)}$ can therefore be seen as a correction factor $C(\alpha, n)$, as outlined in [27].

To acquire an average thickness value, $C(\alpha, n)$ is integrated over the full aperture angle

$$C(\alpha_{\text{apt}}, n) = \frac{1}{\alpha_{\text{apt}}} \int_0^{\alpha_{\text{apt}}} \frac{\cos \beta}{\cos \alpha} d\alpha. \quad (12)$$

The formula for the sample thickness a is then dependent on the sensor's NA and Eq. 11 is written as

$$a = n(\Delta z - d_1 + d_2) \cdot C(\text{NA}, n). \quad (13)$$

With knowledge of the refractive index and the numerical aperture, the sample thickness can therefore be determined. By measuring the sensor's z-axis displacement, the measurement of samples much thicker than the nominal CCS measuring range is possible. The theoretical maximum sample thickness then derives to

$$a_{\text{max}} = n(m_d + m_r). \quad (14)$$

Comparing this result to Eq. 1, it can be seen that the maximum measuring thickness still depends on n , which is fixed for a specific sample, but is greatly increased since m_d is typically about 7 times larger than m_r [24]. It should be noted that the equations above are derived for the case of a flat sample. For samples exhibiting strong curvatures, a closer look at the refraction at the boundary surfaces is necessary.

III. SYSTEM PROTOTYPE DESIGN

A. System components

In order to demonstrate the mechatronic range extension of CCS thickness sensing, a prototype setup is designed. A fixed-bridge above an XY-positioning system is chosen as basis for the mechanical design. The bridge provides sufficient rigidity for the z-axis drive system with the CCS and enables a stable mounting of the different components. Three stepper motors in combination with linear rails and ball bearing slides provide movement in all three dimensions. The motion of the XY-positioning system and the CCS is observed by interferometric sensors (IDS3010, Attocube Systems AG, Munich, Germany) with a resolution in the sub-nanometer range. The constructed prototype is depicted in Figure 5.

The XY-positioning system consists of two stacked linear axes guided by ball bearing slides on linear rails, depicted in Figure 6. Two flat mirrors are mounted to the sides of the positioning system in order to reflect the infrared light beams emerging from the interferometric sensors, which are aligned so that their beams would intersect with the optical axis of the

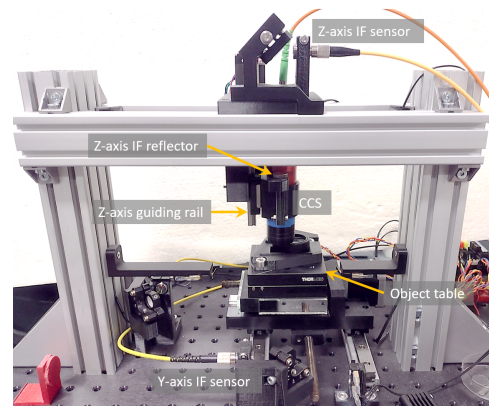


Fig. 5. Picture of the experimental setup using a cartesian coordinate system. The XY-positioning system is moving the sample in two dimensions. The vertically mounted confocal chromatic sensor (CCS) can be moved along the z-axis. Interferometric sensors measure displacement in all three dimensions.

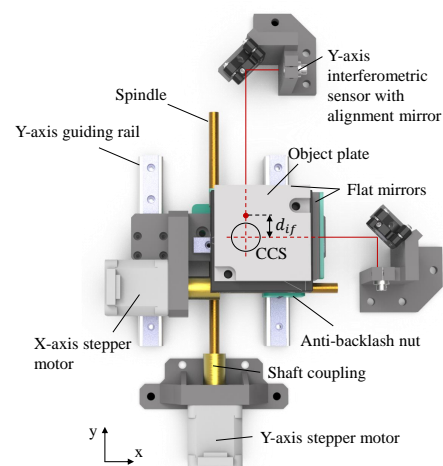


Fig. 6. Alignment of interferometric sensors and mirrors on the XY-positioning system. The virtual intersection of the interferometer beams underneath the CCS is indicated on the object plate. The red dot indicates the optical axis of the z-axis interferometric sensor, which is shifted by $d_{if} = 20$ mm from the central intersection due to constructional reasons.

CCS in one point, thus reducing potential measurement errors following Abbe's Principle [28].

The confocal chromatic sensor model IFS2405-0.3 (Micro-Epsilon, Ortenburg, Germany) is chosen for the prototype setup, as it offers a high lateral resolution (spot size of $6 \mu\text{m}$) at the cost of only $300 \mu\text{m}$ measurement range with an NA of 0.6. It is mounted vertically on a ball bearing slide and is guided by a linear rail along the z-axis actuated by a stepper motor via a trapezoidal spindle. The z-axis interferometric sensor keeps track of the CCS movement to effectively realize an extension of the CCS measuring range. To reflect the interferometer

beam, a circular mirror is mounted to the adapter part as close as possible to the confocal sensor, in order to minimize potential Abbe errors in the z-axis measurement.

The stepper motors are driven by three TMC2130 motor drivers (Trinamic, Hamburg, Germany), which are connected to a controller board (SKR v1.3, Big Tree Technology Co., Guangdong, China). Considering the spindle pitch of 1.5 mm and the controller's micro-stepping functionality, (256 microsteps per full step), a nominal step resolution of 34 133 steps/mm is reached. The motors are open-loop controlled and the displacement measured by the interferometric sensors is processed to evaluate experimental results. On the board itself, the Marlin firmware is installed, which uses a derivative of G-code as control language.

B. Measurement process

The sample is measured in a step-by-step fashion, as illustrated in Figure 7. After each step, the CCS controller unit acquires the distance and thickness information, while the sensor data of the interferometers in all three axes is also logged. The depicted measuring pattern for XY-positioning ensures that a possible spindle backlash only appears in the border regions of the imaged area and does not impair the measurement of the desired region of interest. The system is capable of measuring about 2 to 5 points per second, depending on the chosen step size. For the extended thickness measurement, the CCS is further moved up and down in each measurement point by Δz to acquire bottom surface data. With

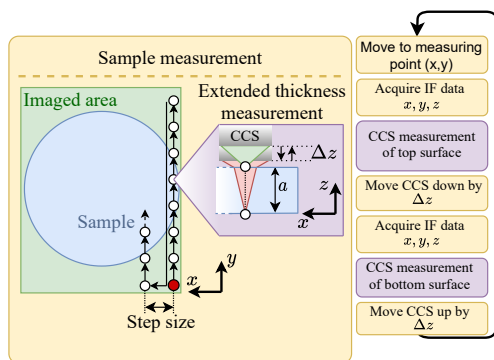


Fig. 7. Illustration of measurement process for extended thickness measurement. At each measuring point, the CCS is moved down by Δz to measure the distance to the bottom surface while the interferometer (IF) data is acquired. Afterwards the CCS is moved up again and the sample is repositioned using the linear stages for the next surface measurement.

Eq. 13, the necessary z-displacement can be roughly derived as

$$\Delta z \approx \frac{a}{n}, \quad (15)$$

meaning the measuring time depends on the sample's thickness a and its refractive index n . A thickness measurement on an area of 1 mm^2 of a 1 mm thick sample, measured with a step

size of $50 \mu\text{m}$, including CCS movement, then takes about 5 times longer than one conventional top surface measurement. However, for a conventional thickness measurement an additional surface measurement of the bottom sample side would still be necessary.

IV. EXPERIMENTAL RESULTS

In order to validate the working principle of the implemented range extension for thickness measurements, experiments on different samples are performed. First, the thickness of multiple BK7-glass windows of well-known thicknesses is measured with the range-extended CCS. Second, a USAF resolution test target is measured upside-down and in proper orientation to verify whether the lateral resolution (determined by the spot size) is preserved in the extended measurement regime. Additionally, the accuracy of the system is verified by measuring the corner points of a bar target. A rigid contact lens is measured and the repeatability is determined. Finally, the shape of a PMMA lenslet array is measured from the backside to demonstrate the combination of high lateral resolution and extended measurement range.

A. Range extension validation

The thickness of three optical glass windows (WBK-251/252/253 BK7, UQG Optics, Cambridge, United Kingdom) is measured. The nominal thicknesses d_{nom} are listed in the first column of Table I.

In order to verify these specifications, the real thickness d_{real} is determined in a preliminary experiment as follows: First, the distance to the empty object table is measured. After placing the sample underneath the sensor, the CCS is moved upwards until the distance to the sample surface can be acquired. By considering the travelled distance Δz and subtracting the difference of the measured distance values, the sample thickness d_{real} is determined, which serves as a reference for the thickness measurement using the range extension, denoted as d_{meas} . The thickness measurement is conducted as follows: After each measured point on the top surface (d_1), the CCS is moved down as shown in Figure 4 and iteratively repositioned until the distance value d_2 measured from the bottom surface lies within a range of $\pm 0.5 \mu\text{m}$ around d_1 . Thus, Eq. 13 simplifies to

$$d_{\text{meas}} = n \cdot \Delta z \cdot C(\text{NA}, n) \quad (16)$$

with the height difference in the z-interferometer data given by Δz and the refractive index $n = 1.5168$ of the optical windows. Numerical integration of Eq. 12 yields a correction factor

$$C(\text{NA}, n) = C(0.6, 1.5168) = 1.0443. \quad (17)$$

The measurement results are listed in Table I. The 5 mm test case is realised by stacking the 2 mm sample on top of the 3 mm glass window. From this result, a range extension by a factor of $d_{\text{real}}/m_r = 5.187 \text{ mm}/0.3 \text{ mm} = 17.29$ can be determined. In Figure 8 the relative errors of the

TABLE I

EXTENDED MEASUREMENT PERFORMED ON TRANSPARENT SAMPLES. 50 MEASUREMENTS ARE CARRIED OUT FOR THE LISTED MEAN (μ) AND STANDARD DEVIATION (σ) VALUES.

d_{nom}	d_{real}	$d_{\text{meas}}(\mu) \pm \sigma$	rel. error (%)
1 mm	1.085 mm	$1.099 \pm 4.4 \times 10^{-4}$ mm	1.30 %
2 mm	2.099 mm	$2.152 \pm 5.2 \times 10^{-4}$ mm	2.54 %
3 mm	3.088 mm	$3.176 \pm 1.7 \times 10^{-3}$ mm	2.86 %
5 mm	5.187 mm	$5.367 \pm 2.55 \times 10^{-3}$ mm	3.48 %

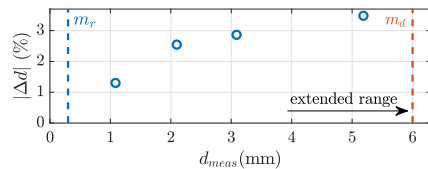


Fig. 8. Relative error Δd with increasing sample thickness d . The nominal CCS measuring range m_r and the theoretical limit of the extended measuring range m_d are also shown.

conducted thickness measurements are shown. The nominal CCS measuring range m_r and the measuring distance m_d are also indicated. Notably, the relative error rises slightly with increasing sample thickness, where most part of the CCS light path lies inside the sample. A more distinct correction approach tackling remaining systematic errors by considering the light distribution in air and in the sample may improve this result.

B. Evaluation of lateral resolution and accuracy

In general, the achievable lateral resolution is related to the spot size of the CCS, which depends on the numerical aperture, the size of the pinhole and the mean focal distance of the objective [22]. In this case, a spot size of about $6 \mu\text{m}$ is specified for the used CCS, which gives a first indication about the size range of the lateral resolution. In order to experimentally determine the imaging resolution of the setup, a resolution test target (1R3L3S1P-Positive 1951 USAF Test Target, Thorlabs Inc., New Jersey, United States) is used. The result of an intensity measurement of the center area ($0.3 \times 0.3 \text{ mm}^2$) of the USAF target is depicted in Figure 9a and 9b. The last element which is clearly resolved is element 4 of group 7, encased by the red rectangle. From this result, the lateral resolution for surface measurements can then be determined to be $R_{\text{lat}} = 2^{(7+\frac{3}{5})} = 203.187 \text{ lp/mm}$, which is equivalent to a line width of $2.46 \mu\text{m}$, about half of the spot size of $6 \mu\text{m}$.

In order to determine the achievable lateral resolution of the proposed thickness measurement principle, depicted in Figure 3c, the USAF target is flipped upside down and the CCS distance to the sample is adjusted, until the bottom surface lies in the middle of the sensor's measuring range. On an area of $150 \times 60 \mu\text{m}^2$ containing group 7, an intensity measurement

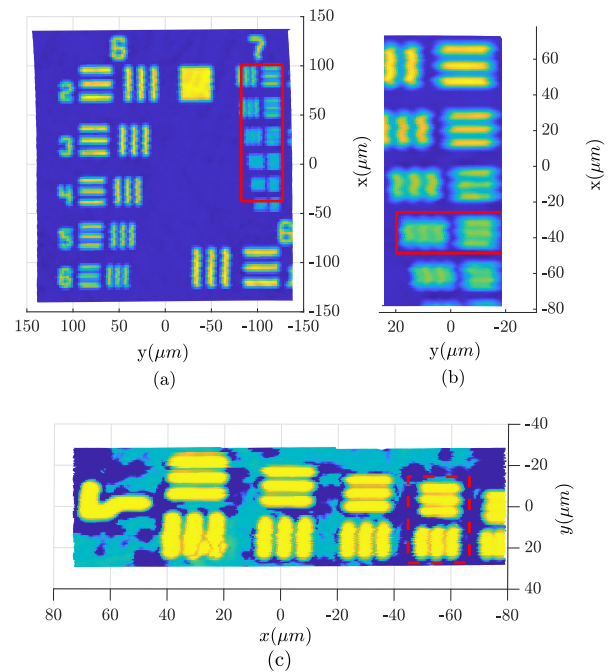


Fig. 9. Intensity measurement on USAF Resolution Test Target. (a) The center area of the target is measured with a step size of $2.5 \mu\text{m}$. Group 7 (in red) is measured with a finer step size of 750 nm . (b) Three distinguishable lines are still visible in element 4 (small red box), determining the lateral resolution to $2.46 \mu\text{m}$. (c) The USAF target is flipped upside-down and the CCS is moved down until the bottom surface lies again in the middle of the nominal measuring range. Group 7 is measured through the sample thickness of 1.5 mm with a lateral step size of 750 nm , showing that the same lateral resolution as in the nominal surface measurement can be achieved with the proposed thickness measurement.

with a step size of 750 nm is conducted, with the result depicted in Figure 9c. Between the vertical bar elements on the left side, an irregular intensity patch is visible, which is probably caused by dust on the resolution target, distorting the intensity measurement. Notably, the imaging resolution on the bottom side of the 1.5 mm thick target is determined by the same element as in the previous case (indicated by the red box), confirming the preservation of the lateral resolution for thickness measurements.

In order to verify the accuracy of the system an intensity measurement with a step size of $2 \mu\text{m}$ is conducted on the test target (group -2 , element 2) with a specified area of $8.909 \times 8.909 \text{ mm}^2$. The accuracy is then calculated for the XY-plane as

$$\varepsilon_{x,y} = \frac{d_{x,y}^{\text{meas}} - d_{x,y}^{\text{actual}}}{d_{x,y}^{\text{actual}}} \quad (18)$$

with $d_{x,y}^{\text{meas}}$ being the measured length of the element for x and y directions, respectively, and $d_{x,y}^{\text{actual}}$ being the spec-sheet

value of the target length. The resulting errors then amount to

$$\varepsilon_x = \frac{8.83 \mu\text{m}}{8909 \mu\text{m}} = 0.09\%, \quad \varepsilon_y = \frac{10.96 \mu\text{m}}{8909 \mu\text{m}} = 0.12\%, \quad (19)$$

for each axis.

C. Shape measurement of contact lens and microlens array

The system's repeatability is evaluated by conducting 20 diagonal line measurements with a step size of $50 \mu\text{m}$ across the surface of a rigid contact lens, depicted in Figure 10. The CCS is moved along the z-axis in order to keep the lens within the sensor's measuring range in each measuring point. The standard

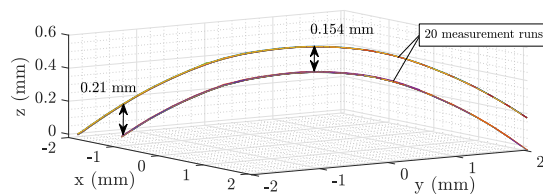


Fig. 10. 20 measurement runs are conducted diagonally across a rigid contact lens with a step size of $50 \mu\text{m}$ in order to evaluate the systems repeatability in 3D space. At each measuring point, the thickness is measured while the CCS distance to the sample is adjusted frequently.

deviations are calculated to $\sigma_{xy} = 3.6 \mu\text{m}$ for XY-positioning and $\sigma_z = 1.8 \mu\text{m}$ for the combined measurement of top surface points with the CCS and the z-axis interferometer.

In order to determine the systematic error introduced by the z-axis movement of the CCS in each step, a surface measurement of a flat, inclined sample is conducted two ways. First, a measurement is carried out along the rising slope utilizing the whole spec-sheet measurement range of $300 \mu\text{m}$ of the CCS - the fixed CCS measurement scheme. Then, the same measurement is performed while the CCS distance to the sample is adjusted in every measuring point to keep the surface in the middle of the CCS spec-sheet measuring range. Between the resulting two slope measurements, an angular deviation of 0.0472° can be observed, resulting in an error of $0.826 \mu\text{m}/\text{mm}$. These findings enable a systematic error compensation of the system.

Microlens arrays with a lens pitch in the micron range are used in Shack-Hartmann sensors for wavefront measurements [29]. Well-established methods such as microdroplet jetting, microplastic embossing and precision machining are in use for the manufacturing of microlens arrays, however, the product quality still needs to improve [30].

In order to validate the proposed thickness measurement principle with maintained high lateral resolution, a lenslet array made out of PMMA (MLA1, Thorlabs Inc., United States) with a nominal thickness of 1.2 mm and a refractive index of 1.4906 is measured from the backside. A line measurement is performed, depicted in Figure 11, measured with a lateral step size of $5 \mu\text{m}$. The measured data from the bottom surface is corrected with Eq. 16 in order to create the line plot. The encircled area shows

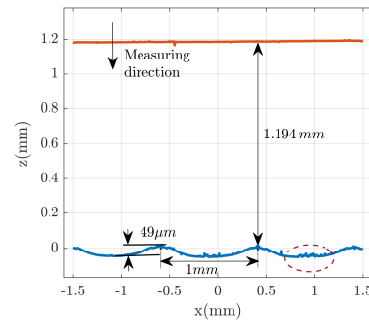


Fig. 11. Line measurement from the backside of a 1.2 mm thick PMMA lenslet array, measured with a step size of $5 \mu\text{m}$.

surface artifacts with a peak-to-peak value of about $10 \mu\text{m}$. The single lens height amounts to $49 \mu\text{m}$, which corresponds well to the specified value of $46.9 \mu\text{m}$ in the data sheet. In Figure 12

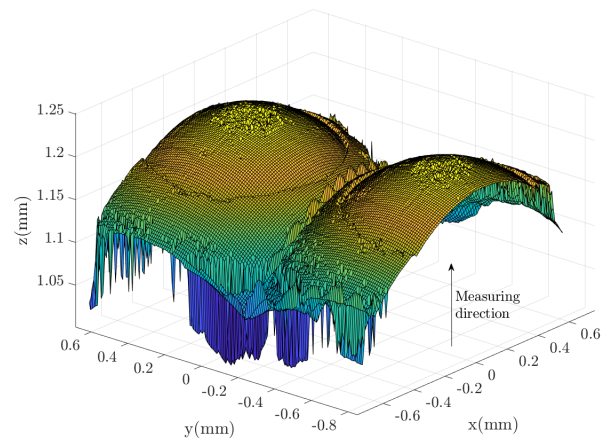


Fig. 12. An area of $1.5 \times 1.5 \text{ mm}^2$ of a 1.2 mm thick PMMA lenslet array is measured from the backside with a step size of $10 \mu\text{m}$. In the center area, surface defects, caused by the manufacturing process, are clearly visible.

a 3D image of the measured section is depicted. For visibility reasons, only the bottom surface area is shown. In the center lens area, the same surface defects as in the line measurement result are visible, which are likely caused by the manufacturing process. Some outliers are visible in the edge region of the individual lenses, probably caused by further surface defects, which are prone to scatter the incoming light [31], leading to signal loss in the CCS measurement.

In summary, axial repositioning of a CCS extends the measuring range by a factor of 17, which is demonstrated by surface and thickness measurements of transparent objects. This proposed approach therefore overcomes the traditional tradeoff between lateral resolution and thickness measuring range.

V. CONCLUSION

This paper presents a strategy to break the tradeoff between the thickness measuring range of a confocal chromatic sensor (CCS) and its lateral resolution, which is determined by the sensor's spot size. By combining the CCS with a linear positioning stage, a mechatronic approach is pursued to effectively extend the measuring range, theoretically only limited by the offset distance of the nominal measuring range from the sensor's aperture. Thus, small lateral structures in the size range of the CCS spot size can be measured on the surface of thick samples from the back side. The measuring range is extended by a factor of 17 and the proposed measurement principle is demonstrated by measuring surface features on a 1.2 mm thick lenslet array from the backside, while maintaining the same lateral resolution of 2.46 μm for thickness measurements as for nominal surface measurements. Future work focuses on improving the correction algorithms for thickness measurements by considering the sample curvature.

ACKNOWLEDGMENTS

The financial support by the Christian Doppler Research Association, the Austrian Federal Ministry for Digital and Economic Affairs, and the National Foundation for Research, Technology and Development, as well as MICRO-EPSILON MESSTECHNIK GmbH & Co. KG and ATENSOR Engineering and Technology Systems GmbH is gratefully acknowledged.

REFERENCES

- [1] L. Zhu, Z. Li, F. Fang, S. Huang, and X. Zhang. "Review on fast tool servo machining of optical freeform surfaces". In: *The International Journal of Advanced Manufacturing Technology* 95.5-8 (Nov. 2017), pp. 2071–2092.
- [2] J. M. Lee, D. Lee, and Y. Baek. "Fabrication of dual-focus dual-layered microlens". In: *Optics Communications* 289 (2013), pp. 69–74.
- [3] J. Chen, L. Mi, C. P. Chen, H. Liu, J. Jiang, and W. Zhang. "Design of foveated contact lens display for augmented reality". In: *Opt. Express* 27.26 (Dec. 2019), pp. 38204–38219.
- [4] H. Liu, Y. Huang, and H. Jiang. "Artificial eye for scopic vision with bioinspired all-optical photosensitivity enhancer". In: *Proceedings of the National Academy of Sciences* 113.15 (2016), pp. 3982–3985.
- [5] K. Choi and H. G. Park. "Smart Reinvention of the Contact Lens with Graphene". In: *ACS Nano* 11.6 (2017), pp. 5223–5226.
- [6] F. Fang, X. Zhang, A. Weckenmann, G. Zhang, and C. Evans. "Manufacturing and measurement of freeform optics". In: *CIRP Annals* 62.2 (2013), pp. 823–846.
- [7] R. Henselmans, L. Cacace, G. Kramer, P. Rosielle, and M. Steinbuch. "The NANOMEFOS non-contact measurement machine for freeform optics". In: *Precision Engineering* 35.4 (Oct. 2011), pp. 607–624.
- [8] H.-L. Du, Z.-Z. Zhou, Z.-Q. Sun, B.-F. Ju, S. Xu, and A. Sun. "Full area covered 3D profile measurement of special-shaped optics based on a new prototype non-contact profiler". In: *Review of Scientific Instruments* 88.6 (2017), p. 065102.
- [9] S. Reichelt, C. Pruss, and H. J. Tiziani. "Absolute interferometric test of aspheres by use of twin computer-generated holograms". In: *Applied Optics* 42.22 (Aug. 2003), p. 4468.
- [10] K. K. Pant, D. R. Burada, M. Bichra, M. P. Singh, A. Ghosh, G. S. Khan, S. Sinzinger, and C. Shakher. "Subaperture stitching for measurement of freeform wavefront". In: *Appl. Opt.* 54.34 (Dec. 2015), pp. 10022–10028.
- [11] M. Brunelle, J. Yuan, K. Medicus, and J. D. Nelson. "Importance of fiducials on freeform optics". In: *Optifab 2015*. Ed. by J. L. Bentley and S. Stoebenau. SPIE, Oct. 2015.
- [12] H. J. Tiziani and H.-M. Uhde. "Three-dimensional image sensing by chromatic confocal microscopy". In: *Appl. Opt.* 33.10 (Apr. 1994), pp. 1838–1843.
- [13] A. F. Forughi, B. Stoeber, and S. I. Green. "Transparency measurement of thin films with one-sided optical access using fluorescence imaging". In: *Appl. Opt.* 56.12 (Apr. 2017), pp. 3359–3364.
- [14] J. Garzón, T. Gharbi, and J. Meneses. "Real time determination of the optical thickness and topography of tissues by chromatic confocal microscopy". In: *Journal of Optics A: Pure and Applied Optics* 10.10 (Sept. 2008), p. 104028.
- [15] S. Niese and J. Quodbach. "Application of a chromatic confocal measurement system as new approach for inline wet film thickness determination in continuous oral film manufacturing processes". In: *International Journal of Pharmaceutics* 551.1 (2018), pp. 203–211. ISSN: 0378-5173.
- [16] M. Agoyan, G. Fournau, G. Cheymol, A. Ladaci, H. Maskrot, C. Destouches, D. Fourmentel, S. Girard, and A. Boukenter. "Toward Confocal Chromatic Sensing in Nuclear Reactors: In Situ Optical Refractive Index Measurements of Bulk Glass". In: *IEEE Transactions on Nuclear Science* 69.4 (2022), pp. 722–730. DOI: 10.1109/TNS.2022.3150221.
- [17] L.-C. Chen, D. T. Nguyen, and Y.-W. Chang. "Precise optical surface profilometry using innovative chromatic differential confocal microscopy". In: *Opt. Lett.* 41.24 (Dec. 2016), pp. 5660–5663.
- [18] H. Duan, S. Morita, T. Hosobata, M. Takeda, and Y. Yamagata. "Profile Measurement Using Confocal Chromatic Probe on Ultrahigh Precision Machine Tool". In: *International Journal of Automation Technology* 15.2 (2021), pp. 225–233.
- [19] P. Chiariotti, M. Fitti, P. Castellini, S. Zitti, M. Zannini, and N. Paone. "Smart quality control station for non-contact measurement of cylindrical parts based on a

- confocal chromatic sensor". In: *IEEE Instrumentation Measurement Magazine* 21.6 (2018), pp. 22–28. DOI: 10.1109/MIM.2018.8573589.
- [20] R. Zhou, D. Shen, P. Huang, L. Kong, and Z. Zhu. "Chromatic confocal sensor-based sub-aperture scanning and stitching for the measurement of microstructured optical surfaces". In: *Opt. Express* 29.21 (Oct. 2021), pp. 33512–33526.
- [21] H. M. Park, U. Kwon, and K.-N. Joo. "Vision chromatic confocal sensor based on a geometrical phase lens". In: *Appl. Opt.* 60.10 (Apr. 2021), pp. 2898–2901.
- [22] R. Leach, ed. *Optical Measurement of Surface Topography*. Springer Berlin Heidelberg, 2011, p. 97.
- [23] M. E. Fuerst, E. Csencsics, C. Haider, and G. Schitter. "Confocal chromatic sensor with an actively tilted lens for 3D measurement". In: *J. Opt. Soc. Am. A* 37.9 (Sept. 2020), B46–B52.
- [24] *Confocal Chromatic Sensors*. Micro-Epsilon. 2021. URL: <https://www.micro-epsilon.de/download/products/cat--confocalDT--de.pdf>.
- [25] M. Kunkel, J. Schulze, M. Kogel-Hollacher, and S. Sprentall. "Non-contact measurement of central lens thickness". In: *International Congress on Applications of Lasers & Electro-Optics*. Laser Institute of America, 2005.
- [26] A. Miks, J. Novak, and P. Novak. "Analysis of method for measuring thickness of plane-parallel plates and lenses using chromatic confocal sensor". In: *Appl. Opt.* 49.17 (June 2010), pp. 3259–3264.
- [27] M. Quinten. "Thickness Determination of Transparent Coatings". In: *PhotonicsViews* 16.3 (May 2019), pp. 68–71.
- [28] E. Abbé. "Meßapparate Für Physiker". In: *Zeitschrift Für Instrumentenkunde* 10 (1890), pp. 446–447.
- [29] B. C. Platt and R. Shack. "History and Principles of Shack-Hartmann Wavefront Sensing". In: *Journal of Refractive Surgery* 17.5 (2001), S573–S577.
- [30] W. Yuan, L.-H. Li, W.-B. Lee, and C.-Y. Chan. "Fabrication of Microlens Array and Its Application: A Review". In: *Chinese Journal of Mechanical Engineering* 31.1 (Feb. 2018).
- [31] D. Yao, P. Nagarajan, L. Li, and A. Y. Yi. "A two-station embossing process for rapid fabrication of surface microstructures on thermoplastic polymers". In: *Polymer Engineering & Science* 47.4 (2007), pp. 530–539.

VI. BIOGRAPHY SECTION



Christian Haider received the MSc. degree in electrical engineering from TU Wien, Austria in 2020. He is currently working towards the PhD degree at the Automation and Control Institute (ACIN) of TU Wien. His primary research interests include mechatronic system design, optical surface metrology, precision engineering and vibration isolation systems.



Martin E. Fuerst is pursuing his PhD in the Advanced Mechatronic Systems Group at the Automation and Control Institute (ACIN) of TU Wien. He received an MSc. degree in Biomedical Engineering and an MSc. degree in Physical Measurement Engineering in 2016 and 2017, respectively. His primary research interests are control theory and measurement techniques, advances in optical displacement sensing, and optical freeform manufacturing and testing.



Matthias Laimer received the B.Sc. degree in electrical engineering and information technology from TU Wien, Austria, in 2020. He is currently pursuing the MSc. degree in energy systems and automation technology with the Automation and Control Institute (ACIN). His main interests are control theory and optical metrology systems, focusing on the development of algorithms for control tasks and measurement processes.



Ernst Csencsics is assistant professor for Metrology Systems in the Advanced Mechatronic Systems group at the Automation and Control Institute (ACIN) of TU Wien. He received an MSc. and a PhD degree (sub auspiciis) in Electrical Engineering from TU Vienna, Austria in 2014 and 2017, respectively. His primary research interests are on high performance mechatronic systems, the development of holistic methods for multidisciplinary system design and integration, opto-mechatronic measurement and imaging systems, precision engineering, and robot-based in-line measurement systems. He received the journal best paper award of IEEE/ASME Transactions on Mechatronics (2018) and the best student paper award at the American Control Conference (2016).



Georg Schitter is Professor for Advanced Mechatronic Systems at the Automation and Control Institute (ACIN) of TU Wien. He received an MSc in Electrical Engineering from TU Graz, Austria (2000) and an MSc and PhD degree from ETH Zurich, Switzerland (2004). His primary research interests are on high-performance mechatronic systems, particularly for applications in the high-tech industry, scientific instrumentation, and mechatronic imaging systems, such as AFM, scanning laser and LIDAR systems, telescope systems, adaptive optics, and lithography systems for semiconductor industry. He received the journal best paper award of IEEE/ASME Transactions on Mechatronics (2018), of the IFAC Mechatronics (2008-2010), of the Asian Journal of Control (2004-2005), and the 2013 IFAC Mechatronics Young Researcher Award. He served as an Associate Editor for IFAC Mechatronics, Control Engineering Practice, and for the IEEE Transactions on Mechatronics.